

Skyrmion flop transition and congregation of mutually orthogonal skyrmions in cubic helimagnets

Sergei M Vlasov^{1,2}, Valery M Uzdin^{1,2} and Andrey O Leonov^{3,4,5}

¹ St. Petersburg State University, St. Petersburg, 198504, Russia

² ITMO University, St. Petersburg, 197101, Russia

³ Chirality Research Center, Hiroshima University, Higashi-Hiroshima, Hiroshima 739-8526, Japan

⁴ Department of Chemistry, Faculty of Science, Hiroshima University Kagamiyama, Higashi Hiroshima, Hiroshima 739-8526, Japan

⁵ IFW Dresden, Postfach 270016, D-01171 Dresden, Germany

E-mail: vlasov@itmo.ru

Received 15 September 2019, revised 21 December 2019

Accepted for publication 21 January 2020

Published 6 February 2020



Abstract

Magnetic chiral skyrmions are particle-like excitations with a topological charge, which are currently considered as promising objects for the next generation of magnetic memory, logic, and neuromorphic devices. In three-dimensional systems, they can form rather complex topological structures. In bulk helimagnets, elongated skyrmion tubes can be ordered either perpendicularly or parallel to an external magnetic field and such configurations coexist in a specific range of fields. We have shown that with an increase in the magnetic field, the transition from perpendicular to parallel ordering in a 3D skyrmion dimer occurs through an intermediate state with mutually orthogonal skyrmion tubes. In the system with three and more skyrmion tubes, we uncovered a surprisingly large diversity of superstructures and systemized the principles of their formation. The nascent conical state is shown to induce the field-dependent switch between favored skyrmion clusters and underlies attracting inter-skyrmion potential. We argue that our numerical simulations on skyrmion clusters are valid in a parameter range corresponding to the A-phase region of cubic helimagnets. Moreover, skyrmionic superstructures constitute a novel concept of spintronic devices based on gapless skyrmion motion along with each other.

Keywords: magnetic skyrmions, chiral magnetism, nanotubes, minimum energy paths

(Some figures may appear in colour only in the online journal)

1. Introduction

In magnetic compounds lacking inversion symmetry, the handedness of the underlying crystal structure induces an asymmetric exchange coupling called the Dzyaloshinskii–Moriya interaction (DMI) [1, 2], which stabilizes long-period spatial modulations of the magnetization with a fixed rotation sense [3, 4]. Within a continuum approximation for magnetic properties, the DMI is expressed by Lifshitz invariants involving first derivatives of the magnetisation \mathbf{M} with respect to the spatial coordinates [5]:

$\mathcal{L}_{ij}^{(k)} = M_i \partial M_j / \partial x_k - M_j \partial M_i / \partial x_k$. Chiral interactions (having the same functional form) may appear also in many other systems: in ferroelectrics with a non-centrosymmetric parent paraelectric phase, non-centrosymmetric superconductors, multiferroics [6–8], or even in metallic supercooled liquids and glasses [9, 10]. In particular, chiral liquid crystals are considered as an perfect model system for probing behaviour of different modulated structures on the mesoscopic scale [11].

In the last years, a renewed interest in non-centrosymmetric condensed-matter systems has been inspired by the discovery

of two-dimensional (2D) localized modulations, commonly called magnetic skyrmions [12–14]. PdFe/Ir (1 1 1) bilayers provide an ideal platform to investigate the internal properties of such 2D isolated skyrmions (IS) [15, 16]. The heavy metal in such thin film systems provides strong spin–orbit coupling responsible for the induced DMI [17]. Tunnel microscope tip can be used for manipulation by skyrmions: it allows to create, destroy, and detect magnetic skyrmions in a particular location on a surface [15]. Stability of 2D skyrmions in PdFe/Ir (1 1 1) systems at arbitrary temperature can be estimated within the framework of transition state theory (TST) [18–20]. Moreover, the magnetisation reversal of small magnetic clusters on the tip of tunnel microscope and lifetime of correspondent magnetic states can be quantitatively estimated within TST on the basis of microscopic Hamiltonian for itinerant electrons [21]. Observed 2D-ISs are surrounded either (i) by the spins parallel to the applied magnetic field what underlies their repulsive interaction [22, 23] or (ii) by the tilted ferromagnetic state in magnets with easy-plane anisotropy (or oblique magnetic fields [24]) what underlies the anisotropic [25] (repulsive [26]) interaction potential and leads to the formation of bimerons [27, 28]. The nanometer size of magnetic 2D-ISs, their topological protection, and low critical currents predicted to set skyrmions into motion opened a new active field of research in memory and logic devices, in which information is carried by skyrmion bits [29, 30].

Three-dimensional (3D) topological magnetic structures are much more diverse than 2D. Bulk magnetic systems enable propagation of skyrmion tubes either along or perpendicular to an applied magnetic field [31, 32]. In the former case, vertical skyrmions (Sk_v) have axisymmetric shape and perfectly blend into the homogeneous state saturated along the field [12, 14, 33]. In the latter case, horizontal skyrmions (Sk_h) represent ruptures of the conical state realized for low values of the field [25, 31, 32, 34, 35].

Just like in the case of 2D-ISs, the character of IS-IS interaction of 3D-ISs is imposed by a surrounding ‘parental’ state, e.g. a state homogeneously magnetized along the field (repulsive inter-skyrmion potential) or a conical phase with the wave vector along the magnetic field (attraction) what immediately enables complex cluster formation with mutually perpendicular arrangement of skyrmions [36, 37]. Such skyrmion superstructures may underlie precursor phenomena (e.g. the A-phase) near the ordering temperatures in chiral B20 magnets (MnSi [38] and FeGe [39]) and to have prospects in spintronics as an alternative to the common 2D-ISs, in particular, as viable elements of artificial neural networks and computing systems [40].

In this paper, we study the mechanisms of the formation of superstructures from skyrmion tubes. These processes can be controlled by an external magnetic field, which changes the ground state of the system and modifies the effective interaction between the tubes.

The remainder of this article is organized as follows. In section 2, we discuss our model Hamiltonian. Within the continuous and discrete models under consideration, only an applied

magnetic field serves as a control parameter. Thus, we introduce different critical values of the field to indicate different regimes of skyrmion–skyrmion interaction. In particular, the field-dependent conical phase allows to favor a particular type of a skyrmion cluster and underlies the strength of the skyrmion coupling and thus the mutual distances between them.

In section 3 we discuss the internal structure of IS tubes parallel and perpendicular to the external magnetic field, depending on the field strength. Such 3D structures were theoretically predicted and experimentally found in magnetic and liquid crystal systems [31, 32].

Following, we consider the dimers of the skyrmion tubes and show that the field-induced transition from the perpendicular to the parallel ordering of the tubes passes through the state with mutually orthogonal tubes. In section 4, we systematize the principles of a field-driven clustering of mutually orthogonal 3D-ISs and closely investigate the cascade of transitions between them. We also indicate that the formulated concepts of skyrmion clustering could be validated in a parameter range corresponding to the A-phase region of cubic helimagnets. We end with a conclusion and outlook, and briefly discuss potential applications of the various magnetic configurations in spintronic devices.

2. Model

The standard model for magnetic states in bulk cubic non-centrosymmetric ferromagnets is based on the energy density functional [3, 4]

$$w = A (\nabla \cdot \mathbf{m})^2 + D \mathbf{m} \cdot (\nabla \times \mathbf{m}) - \mu_0 \mathbf{M} \mathbf{m} \cdot \mathbf{H}, \quad (1)$$

including the principal interactions essential to stabilize modulated states: the exchange stiffness with constant A , Dzyaloshinskii–Moriya coupling energy with constant D , and the Zeeman energy; \mathbf{m} is the unit vector along the local magnetisation $\mathbf{M} = \mathbf{m}M$, and \mathbf{H} is the magnetic field applied along z -axis.

Solutions for skyrmion tubes with the orientations either along or perpendicular to the field (figure 1) are derived by the Euler equations for the energy functional (1) together with the Maxwell equations.

We use reduced values of the spatial variable, $\mathbf{x} = \mathbf{r}/L_D$ with $L_D = 4\pi A/|D|$ being the periodicity of the modulated states. Then, the skyrmion solutions depends only on the value of the normalized magnetic field, $\mathbf{h} = \mathbf{H}/|\mathbf{H}_D|$, where $|\mu_0 \mathbf{H}_D| = D^2/(2AM)$ is the *saturation field* of the conical phase [4, 12].

The twisting magnetisation \mathbf{m} in the skyrmions also matches boundary conditions imposed by the surrounding conical phase. The equilibrium polar and azimuthal angles for the cone phase are expressed in the analytical form [4] as:

$$\theta_c = \arccos(H/H_D), \quad \psi_c = 2\pi z/L_D. \quad (2)$$

Above the critical field $H = H_D$, the cone phase transforms into the saturated state with $\theta = 0$.

Below we use the discretized version of equation (1):

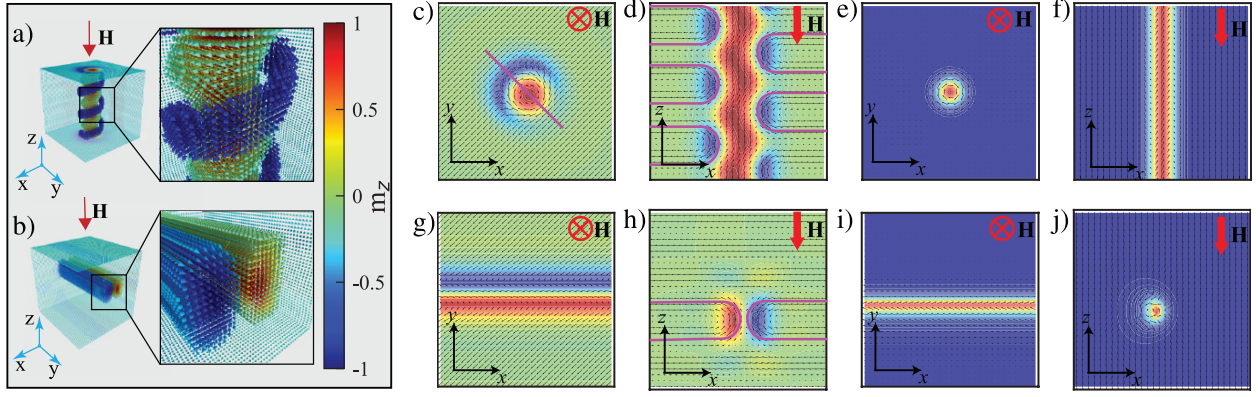


Figure 1. The spin texture of two types of IS, oriented either (a) vertically along the field (Sk_v) or (b) perpendicular to it (Sk_h). In both cases magnetic moments of the conical phase were extracted for illustrative purposes. Insets show magnified regions of the ISs. Red arrows indicate the direction of the applied magnetic field. Sk_h tube is oriented along y-axis for consistency. Magnetic structure of Sk_v , showing its evolution from the non-axisymmetric structure within the spiral phase for $h = 0$ (c) and (d) to the axisymmetric one for $h = 1.0$ (e) and (f). The field is directed parallel to \hat{z} axis. Magnetic structure of Sk_h showing the field-driven evolution for $h = 0$ (g) and (h) (perfect alignment into the spiral state) and $h = 1.0$ (i) and (j). The color plots indicate a \hat{z} component of the magnetisation.

$$E = -J \sum_{\langle i,j \rangle} (\mathbf{S}_i \cdot \mathbf{S}_j) - \sum_{\langle i,j \rangle} \mathbf{D}_{ij} \cdot (\mathbf{S}_i \times \mathbf{S}_j) - \mu \sum_i \mathbf{H} \cdot \mathbf{S}_i, \quad (3)$$

where $\langle i,j \rangle$ denotes pairs of nearest-neighbour sites, \mathbf{S}_i is the unit vectors specifying the direction of the magnetic moment on site i , μ is the value of magnetic moment which is taken to be the same for all sites. Parameters J and vector \mathbf{D}_{ij} determine the magnitude of the exchange and Dzyaloshinsky–Moriya interactions. \mathbf{D}_{ij} ($|\mathbf{D}_{ij}| = D$) is chosen to lie in the plane of the lattice parallel to the vector connecting atomic sites i and j . The magnetic field, \mathbf{H} , is taken to be perpendicular to the plane, i.e. points along the z -axis of the coordinate system.

Value of H_D can be expressed also via parameters of discrete models:

$$H_D = \frac{D^2}{\mu J}.$$

The Dzyaloshinsky–Moriya constant $d = D/J = \tan(2\pi/p)$ determines the period of the modulated structures p , which is a discrete analogue of L_D . Or vice versa, for computational procedures, the modulation period is selected and the corresponding value of d is determined. Dzyaloshinskii–Moriya constant is set to $d = 0.324$ which corresponds to one-dimensional modulations with the period $L_D = 20$. The periodic boundary conditions are implemented along all lateral directions of the 3D computation box.

The energy E of the magnetic configuration will be counted from the energy of the ground state E_0 . Thus, we will use the dimensionless parameter $E_L = (E - E_0)/Jl$, where $l = L/p$, and L is the height of the computational box.

For ISs on a discrete crystal lattice, arguments concerning topological protection, strictly speaking, are not applicable, and here the stability is determined by the height of the barrier separating the system from the state of the uniform magnetisation and the shape of the energy surface in the vicinity of a saddle point on the minimum energy path (MEP) connecting

the states [18, 19, 41]. The magnetic field changes energy landscape and thus the energies of skyrmions as well as their lifetimes at finite temperatures [20]. Moreover, any field-induced change of skyrmion sizes will modify topological Hall effect [42] and in general alter the character of skyrmion–skyrmion interaction.

3. Field-driven skyrmion flop transition and skyrmion dimers

3.1. Internal structure of 3D-ISs

The minimization of the functional (3) was performed with the conjugate gradient descend method with additional Lagrange multipliers (to preserve the length of magnetic moments) for the system with parameters described in the previous section for the computational box of the size $60 \times 60 \times 60$, which corresponds to $L = 3L_D$, and values of the field in the range between $H = 0$ and $H = H_D$.

Only two types of 3D-ISs with the orientation of tubes either along or perpendicular to the field were found within the conical phase of cubic helimagnets. Such a restriction is stipulated by the distinct strategy of ISs to blend into the cone environment. Indeed, Sk_v perfectly blends into the homogeneous state for $H \geq H_D$ (figures 1(e) and (f)) and has smaller energy than Sk_h within the conical state near its saturation field H_D (figures 1(i) and (j)). The internal spin pattern of Sk_v (figure 1(c)) violates the rotational symmetry once placed into the conical phase of bulk cubic helimagnets: the central core region nearly preserves the axial symmetry, whereas the domain-wall region, connecting the core with the embedding conical state is *asymmetric* and acquires a crescent-like shape [36, 37] (pink line in figure 1(c)). This asymmetric profile of the cross-section forms a screw-like modulation along z axis, matching the rotating magnetisation of the cone phase (figure 1(d)).

With the decreasing of magnetic field, however, such inability of Sk_v to match the conical background and the excessive

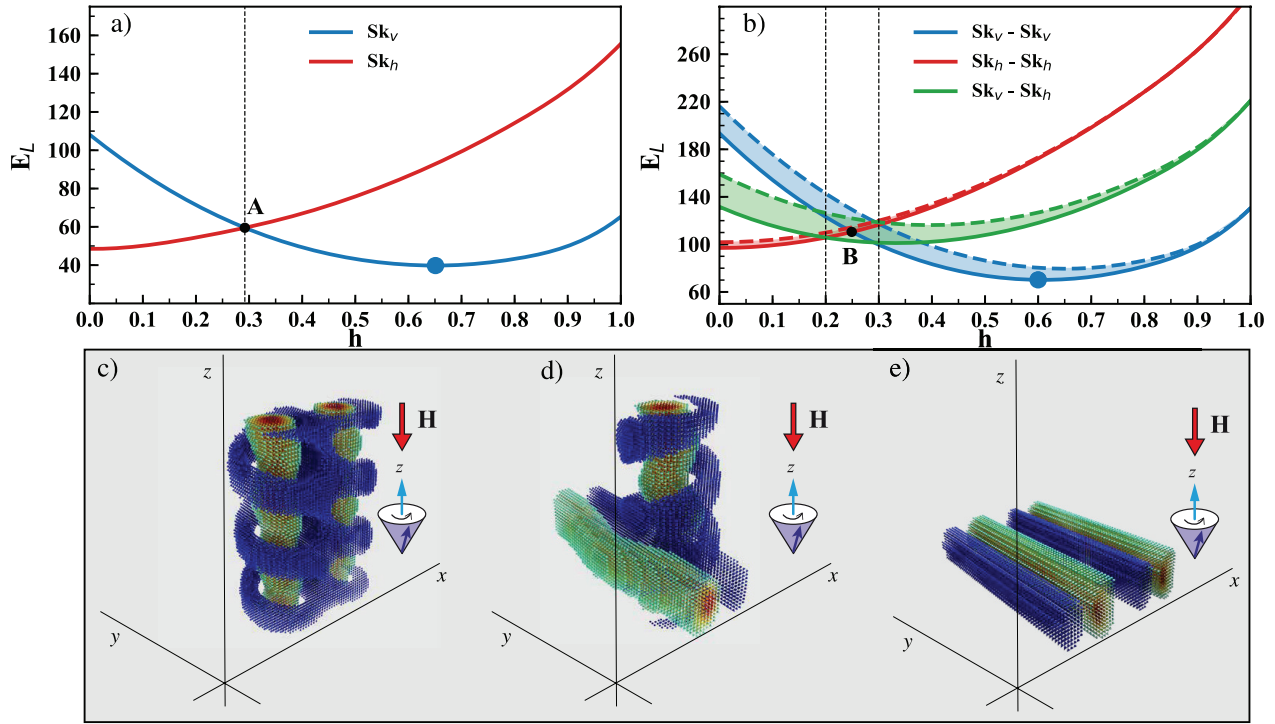


Figure 2. (a) Energies of Sk_V (blue line) and Sk_h (red line) computed with respect to the conical phase. The crossover between two types of ISs (point A in (a)) takes place at $h_A = 0.292$. (b) Energies of two ISs (dashed lines) and coupled skyrmion pairs (solid lines). Since the energy gain due to the clustering is much higher for Sk_V , the crossover field between the pairs $Sk_V - Sk_V$ and $Sk_h - Sk_h$ (red and blue solid lines with an intersection point $h_B = 0.249$) is shifted towards the lower fields. The $Sk_h - Sk_L$ as an ultimate outcome of clustering has higher energy as compared with $Sk_V - Sk_L$ and exhibits no crossover. In the field range $[0.2 \div 0.3]$, an intermediate state $Sk_V - Sk_h$ (green line in (b)) has the minimal energy and thus enables skyrmion superstructures with mutually orthogonal skyrmion constituents. Three types of skyrmion dimers placed into the conical phase are shown in (c)–(e). The spins corresponding to the conical phase were extracted from the spin configurations to illustrate the principle of the compact cluster formation. The cluster formed out of two Sk_V (c) recreates the fragment of a metastable SkL with the homogeneous state between two skyrmions. Such a homogeneous state is formed if the coils of two skyrmions are getting ‘zipped’ together. The same mechanism is applied to the $Sk_V - Sk_h$ cluster (d): Sk_h perfectly fits the gap between the Sk_V ’s coils. In the $Sk_h - Sk_h$ cluster (e), each IS is not distorted or bent, which explains the small energy gain due to the clustering. Furthermore, $Sk_h - Sk_h$ pair exhibits the long-range interaction potential. The magnetic field (red arrow) is applied along $-z$ direction. The color scheme: red cones correspond to the $+z$ direction of the spins and blue—to the $-z$ direction.

energy accumulated in the domain wall region with respect to the conical state lead to the flop transition into the perpendicular orientation of ISs with respect to the field. Indeed, Sk_h perfectly blends into the spiral state (figures 1(g) and (h)) and for $H = 0$ represents a pair of merons with equally distributed topological charge $Q = 1/2$ [34, 35] (red and blue areas in figure 1(h)). Note, that the small anisotropic contributions (e.g. exchange and cubic anisotropies) may stabilize canted ISs with their subsequent smooth reorientation along the field [43].

In what follows, we will operate with the internal structure of 3D-ISs depicted in figures 1(a) and (b) rather than with those in figures 1(c)–(j), i.e. we extract the spin components corresponding to the conical phase (the notion of such a skyrmion structure was introduced in [32]). Then, Sk_V represents a cylinder-like core centred around the magnetisation opposite to the field and a coil with the magnetisation along the field (figure 1(a)). Horizontal skyrmions Sk_h within the same paradigm are displayed as two parallel distorted cylinders centred around the core (red) and the transitional region (blue) with the negative and the positive m_z -component of the magnetisation, correspondingly (figure 1(b)). Two types of skyrmions

undergo different internal transformations with the onset of the homogeneous state for $H > H_D$. Sk_V loses its coil and therefore any distortions of the core, gaining back its axial symmetry. The ‘blue’ counterpart of Sk_h disappears altogether within the ferromagnetic surrounding (figure 1(j)).

Due to the above arguments, the crossover between the two types of ISs (skyrmion flop transition, SFT) takes place for an intermediate value of the field $h_A = 0.292$ (figure 2(a)) and thus enables cluster formation from mutually orthogonal skyrmion tubes.

3.2. Skyrmion dimers composed of Sk_V and Sk_h skyrmions

Skyrmions in helimagnets begin to interact when the distance between them decreases. This interaction can be analyzed by studying dimers from two skyrmion tubes. We consider dimers consisting of two Sk_V s, two Sk_h s as well as Sk_h and Sk_V .

For all three dimers shown in figures 2(c)–(e) the minimization was performed for the elongated computational box of the size $200 \times 60 \times 60$, where ISs were placed close to each other as the initial states.

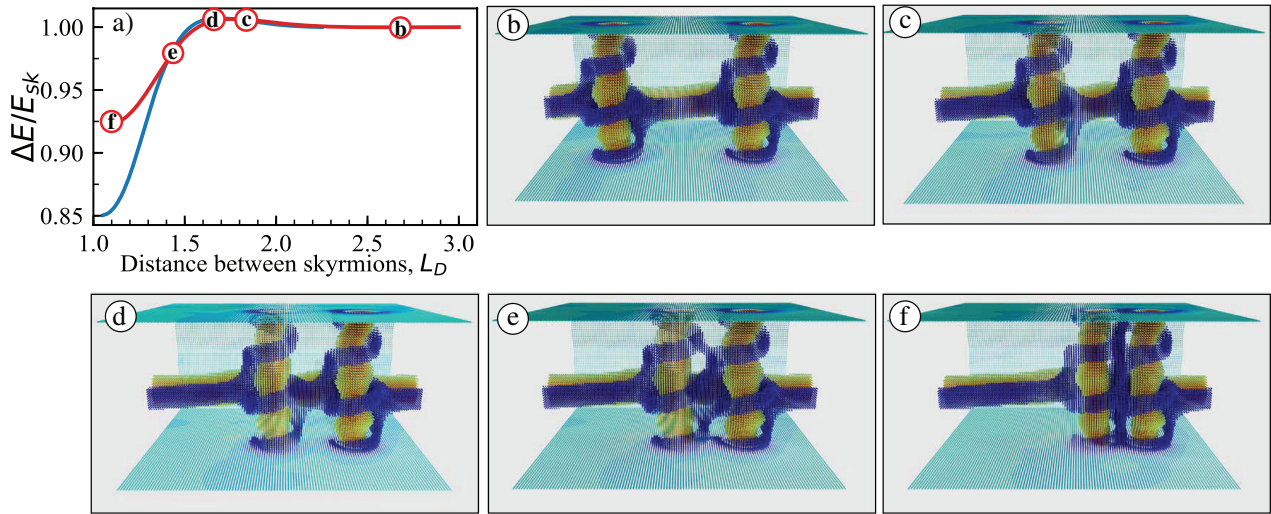


Figure 3. The process of merging of two Sk_v is shown for two ISs (solid blue line in (a)) as well as for two Sk_v gliding along the single Sk_h (solid red line in (a)). The letter marks in (a) correspond to intermediate stages along the minimum energy path that are shown in (b)–(f). In both cases, a small barrier (ca. 1.006 of the energy of the initial state) separates meta-stable states producing ‘zip-locking’ mechanism. When two Sk_v approach each other the energy slightly grows (panels (b)–(d)) and the massive drop of the energy happens when two Sk_v start to merge (panels (e) and (f)). The same pattern is also relevant for the case of two isolated Sk_v . However, the energy gain of coupling is higher for ISs than for Sk_v gliding along the Sk_h .

The cluster formation of vertical skyrmions Sk_v for $h > h_A$ is visualized as a process when the loops of a coil of one IS fill the voids between the loops of another IS (figure 2(c)). By this, the compact skyrmion pair recreates a fragment of a skyrmion lattice (SkL) that within the model (3) is a meta-stable solution: the magnetisation on the way from the center of one IS to the center of another has a rotational fashion as in ordinary axisymmetric skyrmions and thus reduces the energy density in the inter-skyrmion region.

For dimer from Sk_v and Sk_h there are two distinct configurations [32]. Indeed, the transient blue region of the Sk_h may either slide in-between the coils of the vertical skyrmion (configuration shown in figure 2(d)) or just touch the coil of Sk_v if located on the other side. In both states, Sk_h runs along y at the same z coordinate and hence acquires the same polarity.

Cluster formation of horizontal IS Sk_h for $h < h_A$ is illustrated in the figure 2(e)). According to figure 2(b) (red solid line), the configuration with coupled Sk_h (figure 2(e)) is energetically more favourable than two distant Sk_h (dashed red line in (b)) although the energy difference is almost negligible. For other pairs, Sk_v - Sk_h (green lines in figure 2(b)) and Sk_v - Sk_v (blue lines in figure 2(b)), the energy gain due to the clustering may reach as much as 30% compared with the energy of one IS (shaded regions between the dashed and solid lines in figure 2(b)). Note that the cluster Sk_v - Sk_h exhibits the strongest coupling in the field range [0.20, 0.29] and has the lowest energy among three skyrmion dimers. This underlies the field-dependent SFT when the Sk_v s one-by-one flip into the horizontal position.

3.3. Minimum energy path

Skyrmion clusters have lower energy as compared with the decoupled ISs. To enable the cluster formation, however, it is necessary to overcome the energy barriers, which determine

the stability of the bound states. In order to estimate the energy barriers, we have calculated the MEP with the geodesic nudged elastic band method [44].

The MEPs between the states with two vertical ISs (Sk_v) and a pair of coupled Sk_v were calculated for two different configurations: (i) two Sk_v move freely toward each other within the conical phase and (ii) both Sk_v are coupled to the single Sk_h . In both cases the calculations were performed for the box size $100 \times 120 \times 60$. As initial and final configurations we took two distant Sk_v (either coupled to the Sk_h or not) and two coupled Sk_v respectively. Both initial and final states were relaxed prior to the MEP calculation. A linear interpolation with small stochastic noise was used to set intermediate states and construct an initial path between the initial and final configurations with the total number of configurations is 13.

The MEP revealed a small but clearly distinguishable barrier between the states. In figure 3(a) we show MEP for both cases at $h = 0.5$.

We argue that these barriers originate from the necessity to push out the conical surrounding when two skyrmions approach each other what results in the attractive character of the inter-skyrmion potentials. The maximum along both paths exceeds only 1.006 of the initial state energy. Thus, for two Sk_v each having the height L_D , the energy barrier reaches the value 0.8 J and 1.3 J for cases (i) and (ii), respectively. Despite its small value, such a barrier may prevent isolated skyrmions to merge into clusters at low temperatures what opens the opportunity of the thermally assisted cluster formation. For the reverse process, when two Sk_v drift apart from each other, the height of the barrier is higher—18.3 J and 16.8 J, respectively, indicating that coupled skyrmions represent a metastable state. Note, that even though the height of the energy barrier plays a leading role in the stability of the localized states, it is not the only factor. The pre-exponent in the Arrhenius expression, linked to the entropy of the transition state and the initial state also needs to be assessed.

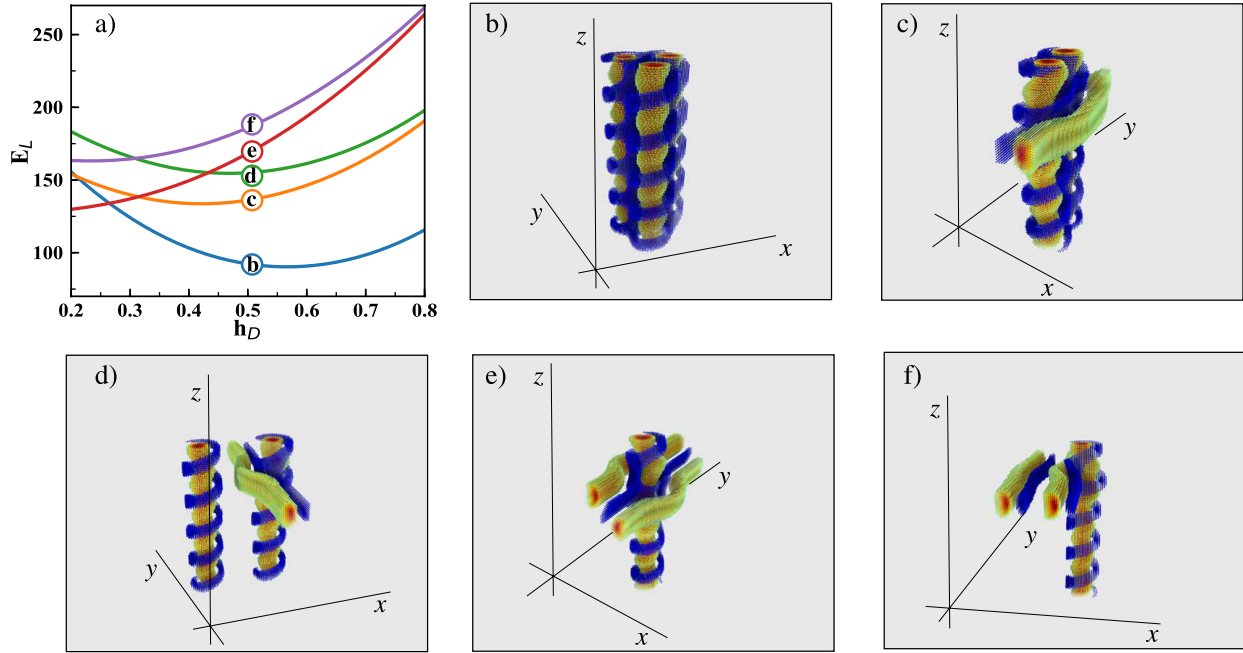


Figure 4. Compact cluster configurations including three isolated skyrmions (b)–(f) at $h = 0.5$. The field dependent cluster energy (a) exhibits field-induced transitions between different skyrmionic trimers.

4. Skyrmion superstructures and the phenomenon of a-phase

So far, pairwise Sk_v - Sk_h interaction was directly identified in thin layers of chiral liquid crystals [32]. Here two theoretically predicted configurations with horizontal skyrmions approaching a vertical isolated skyrmion from both sides were visualized experimentally. Clusters of vertical skyrmions have been observed in thin (70 nm) single-crystal samples of Cu_2OSeO_3 taken using transmission electron microscopy. Horizontal skyrmions are usually observed at zero magnetic field and represent ruptures of the spiral state. Nonetheless, a surprisingly large diversity of skyrmion clusters with mutually orthogonal tubes may be envisioned theoretically (figure 4) and subsequently validated experimentally.

First of all, we notice, that the energy of one Sk_v in figure 2(a) displays a clear minimum realized at $H = 0.651H_D$ with respect to the energy of the conical phase. Any increase of the number of vertical skyrmions in the cluster leads to the shift of the minimum towards lower field values: indeed for two skyrmions, the minimum is realized at $H = 0.608H_D$ (figure 2(b)), for three—at $H = 0.566H_D$ (blue solid line in figure 4(a)). The hexagonal skyrmion lattice (SkL) of Sk_v as an ultimate outcome of clustering has much lower energy as compared with the analogous lattice of Sk_h .

The energy minimum of Sk_v -SkL at $H = 0.4H_D$ corresponds to the region of A-phases of bulk cubic helimagnets near the ordering temperature (e.g. in B20 magnets MnSi [38] and FeGe [39]). Weak interactions such as the ‘softening’ of the magnetisation modulus [39, 45], dipolar interactions, fluctuations [38, 46], etc, may modify the energetic landscape and eventually stabilize the Sk_v -SkL in the A-phase.

According to figure 4(a), the clusters of Sk_v may screen others cluster configurations. In particular, the skyrmion cluster with three Sk_v (figure 4(b)) can be replaced only by the configuration with one Sk_v and two Sk_h (figure 4(e)), which becomes energetically favoured for almost zero field value. Already for four vertical skyrmions in a cluster, no skyrmion flop is observed numerically. The reason lies in the energy gain due to the clustering of Sk_v boosted by every added IS.

In the following, however, we advocate another scenario, so that the universal cluster configurations become apparent. Around the field of skyrmion flop transition (figure 2(a)), the homogeneous nucleation processes of both Sk_v and Sk_h are equally possible. Thus the elongation of torons—spatially localized three-dimensional skyrmions composed of a skyrmion filament of finite length cupped by two Bloch points terminating its prolongation—occurs either along the field direction or in the basal plane xy . Owing to the mutual attracting interaction, skyrmion clusters may create a frozen metastable state, which is defined by the prehistory of the magnetisation processes and acquires higher energy as compared with the Sk_v -SkL. Such a state may include all skyrmion configurations depicted in figure 4 and becomes paramount within A-phases of bulk cubic helimagnets near the ordering temperature (e.g. in B20 magnets MnSi [38] and FeGe [39]). The clusters consisting of the mutually perpendicular skyrmions will then exhibit an entangled pattern since Sk_h do not have any preferable in-plane orientation within the isotropic model (1). On the contrary, an additional cubic anisotropy may align Sk_h along easy directions, e.g. $\langle 100 \rangle$, thus a phase reminiscent a uniaxial model for the Blue Phase II in chiral liquid crystals with symmetry O_2 may occur (see figure B.VIII.12 in [47]).

The structure of skyrmion clusters depicted in figure 4 shows the possibility of gapless skyrmion displacement with respect to each other. In particular, in a ‘skyrmion abacus’ (figures 3(b)–(f)) isolated vertical skyrmions or Sk_v -chains may slide along one horizontal skyrmion. In the configurations of figures 4(e) and (f), horizontal skyrmions may undergo a screw-like rotational motion along one vertical skyrmion. Such examples represent an interesting concept for future spintronic devices.

5. Conclusions

To conclude, we have derived numerical solutions for clusters of 3D skyrmion tubes in external magnetic field. Magnetism of 3D skyrmions is more complicated than 2D analogs from the point of view of their creation, observation, control and manipulation by their structure and properties. Therefore self-organisation of 3D skyrmions and possibility to create from them ordered superstructures using different range of magnetic field and internal skyrmion–skyrmion interactions are of great interest. Even for relatively non-complex structure of skyrmion tubes which can be ordered along (Sk_v) and perpendicular to external magnetic field (Sk_h) their interaction leads to the shift of stability boundaries for differently ordered tubes and their alteration in the region of close location. By the geometrical principles of compact cluster formation, we managed to systematize different types of skyrmion clusters composed from two and three isolated skyrmions.

We have shown that in the simplest case of 3D skyrmion dimer with an increase in the magnetic field the transition from configuration with two horizontal to the configuration with two vertical skyrmion tubes occurs through an intermediate state with mutually orthogonal tubes.

For three skyrmion tubes we found various stable configurations and explained the main principles of their formation. It allows to project superstructures, where for example Sk_v will move along Sk_h like along a rail, which connect two fixed point of the magnetic memory system or another spintronic devices.

The aforementioned skyrmion traits do not only open up new routes for manipulating these quasi-particles in energy-efficient spintronics applications, but also highlight a paramount role of cluster formation within the A-phases of bulk cubic helimagnets near the ordering temperature (e.g. in B20 magnets MnSi and FeGe), the fundamental problem that gave birth to skyrmionics.

Acknowledgments

The authors are grateful to Katsuya Inoue, Istvan Kezsmarki, Maxim Mostovoy, Katia Pappas, Hayley Sohn, and Ivan Smalyukh for useful discussions. This work was funded by Russian Science Foundation (Grant 19-42-06302) and JSPS Core-to-Core Program, Advanced Research Networks (Japan). AOL thanks Ulrike Nitzsche for technical assistance.

ORCID iDs

Sergei M Vlasov  <https://orcid.org/0000-0002-0530-9010>

Valery M Uzdin  <https://orcid.org/0000-0002-9505-0996>

References

- [1] Dzyaloshinsky I 1958 *J. Phys. Chem. Solids* **4** 241–55
- [2] Moriya T 1960 *Phys. Rev.* **120** 91
- [3] Dzyaloshinsky I 1964 *Sov. Phys.—JETP* **19** 960–71
- [4] Bak P and Jensen M H 1980 *J. Phys. C: Solid State Phys.* **13** L881
- [5] Landau L D and Lifshitz E M 1997 *Statistical Physics. Course of Theoretical Physics* vol V (Oxford: Pergamon)
- [6] Bogdanov A and Rößler U 2001 *Phys. Rev. Lett.* **87** 037203
- [7] Bode M, Heide M, Von Bergmann K, Ferriani P, Heinze S, Bihlmayer G, Kubetzka A, Pietzsch O, Blügel S and Wiesendanger R 2007 *Nature* **447** 190
- [8] Wright D C and Mermin N D 1989 *Rev. Mod. Phys.* **61** 385
- [9] Sethna J P 1983 *Phys. Rev. Lett.* **51** 2198
- [10] Sethna J P 1985 *Phys. Rev. B* **31** 6278
- [11] Ackerman P J, Boyle T and Smalyukh I I 2017 *Nat. Commun.* **8** 673
- [12] Bogdanov A and Hubert A 1994 *J. Magn. Magn. Mater.* **138** 255–69
- [13] Yu X, Onose Y, Kanazawa N, Park J, Han J, Matsui Y, Nagaosa N and Tokura Y 2010 *Nature* **465** 901
- [14] Rößler U K, Leonov A A and Bogdanov A N 2011 *Chiral Skyrmionic Matter in Non-Centrosymmetric Magnets (Journal of Physics: Conference Series* vol 303) (Bristol: IOP Publishing) p012105
- [15] Romming N, Hanneken C, Menzel M, Bickel J E, Wolter B, von Bergmann K, Kubetzka A and Wiesendanger R 2013 *Science* **341** 636–9
- [16] Romming N, Kubetzka A, Hanneken C, von Bergmann K and Wiesendanger R 2015 *Phys. Rev. Lett.* **114** 177203
- [17] Jaiswal S et al 2017 *Appl. Phys. Lett.* **111** 022409
- [18] Bessarab P F, Müller G P, Lobanov I S, Rybakov F N, Kiselev N S, Jónsson H, Uzdin V M, Blügel S, Bergqvist L and Delin A 2018 *Sci. Rep.* **8** 3433
- [19] Uzdin V M, Potkina M N, Lobanov I S, Bessarab P F and Jónsson H 2018 *Physica B* **549** 6–9
- [20] Uzdin V M, Potkina M N, Lobanov I S, Bessarab P F and Jónsson H 2018 *J. Magn. Magn. Mater.* **459** 236–40
- [21] Ivanov A, Bessarab P F, Uzdin V M and Jónsson H 2017 *Nanoscale* **9** 13320–5
- [22] Leonov A, Monchesky T, Romming N, Kubetzka A, Bogdanov A and Wiesendanger R 2016 *New J. Phys.* **18** 065003
- [23] Zhang X, Ezawa M and Zhou Y 2015 *Sci. Rep.* **5** 9400
- [24] Schmidt L, Hagemeyer J, Hsu P J, Kubetzka A, Von Bergmann K and Wiesendanger R 2016 *New J. Phys.* **18** 075007
- [25] Leonov A and Kézsmárki I 2017 *Phys. Rev. B* **96** 014423
- [26] Lin S Z, Saxena A and Batista C D 2015 *Phys. Rev. B* **91** 224407
- [27] Yu X, Koshibae W, Tokunaga Y, Shibata K, Taguchi Y, Nagaosa N and Tokura Y 2018 *Nature* **564** 95
- [28] Göbel B, Mook A, Henk J, Mertig I and Tretiakov O A 2019 *Phys. Rev. B* **99** 060407
- [29] Fert A, Cros V and Sampaio J 2013 *Nat. Nanotechnol.* **8** 152
- [30] Finocchio G, Büttner F, Tomasello R, Carpentieri M and Kläui M 2016 *J. Phys. D: Appl. Phys.* **49** 423001
- [31] Leonov A O, Bogdanov A N and Inoue K 2018 *Phys. Rev. B* **98** 060411

- [32] Sohn H R O, Vlasov S M, Uzdin V M, Leonov A O and Smalyukh I I 2019 *Phys. Rev. B* **100** 104401
- [33] Nagaosa N and Tokura Y 2013 *Nat. Nanotechnol.* **8** 899
- [34] Müller J, Rajeswari J, Huang P, Murooka Y, Rønnow H M, Carbone F and Rosch A 2017 *Phys. Rev. Lett.* **119** 137201
- [35] Ezawa M 2011 *Phys. Rev. B* **83** 100408
- [36] Leonov A, Monchesky T, Loudon J and Bogdanov A 2016 *J. Phys.: Condens. Matter* **28** 35LT01
- [37] Loudon J C, Leonov A, Bogdanov A, Hatnean M C and Balakrishnan G 2018 *Phys. Rev. B* **97** 134403
- [38] Mühlbauer S, Binz B, Jonietz F, Pfleiderer C, Rosch A, Neubauer A, Georgii R and Böni P 2009 *Science* **323** 915–9
- [39] Wilhelm H, Baenitz M, Schmidt M, Rößler U, Leonov A and Bogdanov A 2011 *Phys. Rev. Lett.* **107** 127203
- [40] Prychynenko D, Sitte M, Litzius K, Krüger B, Bourianoff G, Kläui M, Sinova J and Everschor-Sitte K 2018 *Phys. Rev. Appl.* **9** 014034
- [41] Lobanov I S, Jónsson H and Uzdin V M 2016 *Phys. Rev. B* **94** 174418
- [42] Denisov K, Rozhansky I, Potkina M N, Lobanov I S, Lähderanta E and Uzdin V M 2018 *Phys. Rev. B* **98** 214407
- [43] Bannenberg L J, Wilhelm H, Cubitt R, Labh A, Schmidt M P, Lelièvre-Berna E, Pappas C, Mostovoy M and Leonov A O 2019 *NPJ Quantum Mater.* **4** 11
- [44] Bessarab P F, Uzdin V M and Jónsson H 2015 *Comput. Phys. Commun.* **196** 335–47
- [45] Leonov A O and Bogdanov A N 2018 *New J. Phys.* **20** 043017
- [46] Buhrandt S and Fritz L 2013 *Phys. Rev. B* **88** 195137
- [47] Oswald P and Pieranski P 2005 *Nematic and Cholesteric Liquid Crystals: Concepts and Physical Properties Illustrated by Experiments* (Boca Raton, FL: CRC Press)